Indian Journal of Engineering & Materials Sciences
Vol. 30, October 2023, pp. 729-734
DOI: 10.56042/ijems.v30i5.6899

# Nd Modified $BiFeO_3$ Perovskites: Investigations on their Structural, and Magnetic Properties

Sourabh Sharma[a], Garima[b], Ashok Kumar[b*], & O P Thakur[a,]

[a]Materials Analysis and Research Laboratory, Netaji Subhas University of Technology, New Delhi 110 078, India

[b]Nano Research Laboratory, Deenbandhu Chhotu Ram University of Science & Technology, Haryana 131 039, India

*Received: 9 August 2023; Accepted: 26 September 2023*

The present work focuses on the examination of the structural and magnetic characteristics of $Bi_{1-x}Nd_xFeO_3$ ($0 \leq x \leq 0.12$) nanoparticles prepared using an efficient wet chemical method, Pechini's modified sol-gel route via auto combustion. $BiFeO_3$ (BFO) is a perovskite multiferroic material which is generally termed as $ABO_3$ where A is Bi or any Rare earth element and B is usually $Fe^{3+}$ or $Mn^{3+}$are looked with great hopes due to its wide possible potential applications such as data storage devices, sensors, $Na^+$ion batteries, spintronics, and magnetoelectric devices. The BFO has sometimes termed a futuristic semiconductor material as a replacement for Silicon by the scientific community. The synthesis process of the nanoparticles involves obtaining the pristine single-phase Bismuth Ferrite (BFO) followed by $Nd^{3+}$ substitutions at the Bi-site to investigate the effects of $Nd^{3+}$ doping in the perovskite system. Characterization techniques such as X-ray diffraction (XRD) are performed in order to confirm the formation of single-phase materials with the desired crystal structure and phase purity.High-Resolution Transmission Electron Microscopy (HRTEM) reveals the formation of distorted rhombohedral structures of NPs with average particle sizes ranging between 18 nm to 50 nm. The magnetic properties are evaluated using a vibrating sample magnetometer (VSM) and Electron Spin Resonance (ESR) to assess the influence of $Nd^{3+}$ doping on the magnetic behavior of the nanoparticles. The experimental results demonstrate the significant impact of $Nd^{3+}$ doping on the magnetic ordering and saturation magnetization of $BiFeO_3$. This research contributes valuable insights into the structural and magnetic properties of Nd-doped BFO nanoparticles, paving the way for the development of advanced magnetoelectric devices with enhanced magnetic functionality.

**Keywords:** Bismuth Ferrite (BFO), Multiferroics, Rare earth doped BFO, ME memory devices

## 1 Introduction

Multiferroics are materials with two or more primary ferroic (Ferroelectric, Ferromagnetic, or Ferroelastic) properties co-existing in the same phase. Among the multiferroics class, materials with both ferroelectric and ferromagnetic properties in which spontaneous magnetization and polarization can be reoriented by an applied magnetic and electric field respectively, are highly studied due to their potential applications for manufacturing of Magneto-Electric Memories, sensors, actuators, transistors, photocatalysts, energy storage devices, and spintronics[1,2]. Since the magnetic/ferroelectric transition temperatures of the majority of single-phase multiferroic materials, including rare earth manganites, are considerably lower at room temperature, their application is restricted to room temperature. $BiFeO_3$ (BFO) stands out from the other multiferroics because it has magnetic and ferroelectric transition temperatures that are significantly higher than room temperature. Bismuth ferrite has a rhombohedral symmetry and an R3c space group with a magnetic Néel temperature of 643 K, while its ferroelectric Curie temperature is 1103 K[3]. Typically, multiferroics are synthesized in perovskite oxides ($ABO_3$) through the production of ferroelectricity from the supposedly lone-pair stereochemical activity on the large cation at the A-site, subsequently followed by the small magnetic cation at the B-site. Ferroelectricity and G-type antiferromagnetism mechanisms in BFO are caused by the aberrations of the lone pair on the $Bi^{3+}$ $6s^2$ ion and the local spin order of $Fe^{3+}$. $Fe^{3+}$ ions create a cycloidal spiral spin structure along the cubic [111] positioning with a 62 nm spin periodicity. BFO has an intriguing possibility for technological use due to the high AFM Néel temperature and ferroelectric Curie temperature[3]. Ions' magnetic moments rotate in a direction that corresponds to the route of the direction of propagation of a modulated wave in a plane that is

*Corresponding author (E-mail:ashokkumar.phy@dcrustm.org)

normal to the hexagonal base plane of BFO. The modulation prevents the emergence of linear magnetoelectric effect and weak ferromagnetism. Even after having a number of characteristic properties, the synthesis of pure single-phase BFO remains a difficult problem for researchers, due to the occurrence of impurity phases such as $Bi_2Fe_4O_9$ and $Bi_{25}FeO_{40}$ at higher temperatures. Additionally, it becomes very difficult to prevent the volatile behaviour of Bi at high temperature[5]. Certainly, doping the A-site with RE elements like Tb, Pr, Nd, Ru, Sr, and Sm adequately inhibits the growth of impurity phases and defects. The doped elements influence the spatially modulated spiral spin arrangement of the BFO, and it is feasible to slightly improve its magnetic behavior in this way. Several research papers are on doping the B-site in Bismuth Ferrite with transition metals, including Co, Cr, Ti, Mn, and Zn, to enhance magnetoelectric characteristics. It has been reported that the substitution of RE ions at the A-site and transition metal ions at the B-site simultaneously results in enhanced magnetic and electrical properties[1]. The rare earth substitution at Bi site is one technique to customize the spin structure and improve electrical properties because it has a different ionic radius from other rare earth (RE) elements[6]. In order to establish the influence of $Nd^{3+}$ substitution at $Bi^{3+}$ site on the structural and magnetic properties our work has been carried out with a systematic study on the $Bi_{1-x}Nd_xFeO_3$ ($0 \leq x \leq 0.12$) nanoparticles prepared by the Pechini's modified sol-gel auto combustion route[4]. To confirm the crystalline structure and phase purity X-Ray diffraction (XRD) has been performed by using PANalytical X'pert PRO X-ray powder diffractometer with $CuK_\alpha$ radiation ($\lambda$ = 1.54 Å)and the HRTEM is done with TEITechnai TF-20 operating at 200kV. The magnetic factors have been calculated by utilizing Microsense ADE-EV9 for ±10KOe field to get M-H curve and the electron spin resonance (ESR) study of the synthesized NPs is done by using a Bruker A300 instrument, with an operating microwave frequency of 9.5 GHz.

## 2 Materials and Methods

Nanoparticles of Neodymium-doped bismuth ferrite ($Bi_{1-x}Nd_xFeO_3$, x=00.03, 0.06, 0.09, 0.12) were produced using a modified version of Pechini's sol-gel process and followed by the auto-combustion[7]. Precursors used in the synthesis were of the following purities and reagent loads: $Bi(NO_3)_3.5H_2O$ (SRL, Purity 98.5%), $Fe(NO_3)_3.9H_2O$ (SRL, Purity 98%), and $Nd(NO_3)_3.6H_2O$ (SRL, Purity 99.9%). These precursors are subsequently dissolved in 20 ml of DW using the correct stoichiometry ratios in individual beakers using the magnetic stirrer for 15 minutes. In addition, 50 ml of distilled water was taken in a separate beaker and the dissolved precursors are mixed in the beaker dropwise through a burette. To this homogeneous solution, 10-12 grams of anhydrous Citric acid ($C_6H_8O_7$) as a chelating agent is added. To neutralize the solution by maintaining 7 pH value, Liq. $NH_3$ (25% concentration) is now supplemented in the mixture. The solution was then placed on stirrer for four to five hours while the hot plate magnetic stirrer's temperature was maintained at 80 degrees Celsius, at this point, the solution had solidified into a gel. The gel is then kept on a hot plate at 300°C temperature to start the auto-combustion process, this results in the raised yellowish ash being obtained which is crushed into fine powder. In order to obtain the nanoparticles of Nd-doped BFO, the powder was annealed in furnace at 600°C for 4 hrs with a constant rate of heating at5°C /min as shown in Fig. 1.

## 3 Results and Discussion

### 3.1 XRD (X-Ray Diffraction)

The diffraction measurement was conducted within the range of 20° to 70°, with a running rate of 2° per minute. The confirmation of phase formation was accomplished using JCPDS card no. 71-2494. Additionally, the crystallite size, interplanar spacing, and lattice parameters were formulated by applying Debye-Scherrer equation and Bragg's equation. For determining the crystallite sizes of the prepared nanoparticles, the Debye-Scherrer equation was employed:

$$D = \frac{k\lambda}{\beta \cos\theta} \quad \ldots (1)$$

In eq(1), k represents the shape factor (0.89), $\beta$ denotes FWHM, $\lambda$ stands for the wavelength of the X-rays, and $\theta$ represents the Bragg's angle. The calculation of interplanar spacing was based on Bragg's equation: $2d_{hkl}\sin\theta_{hkl} = n\lambda$. Moreover, the dislocation density was determined using the equation:

$$\delta = \frac{1}{D^2} \quad \ldots (2)$$

Analysis of the diffraction peaks revealed the presence of the rhombohedral phase as the primary

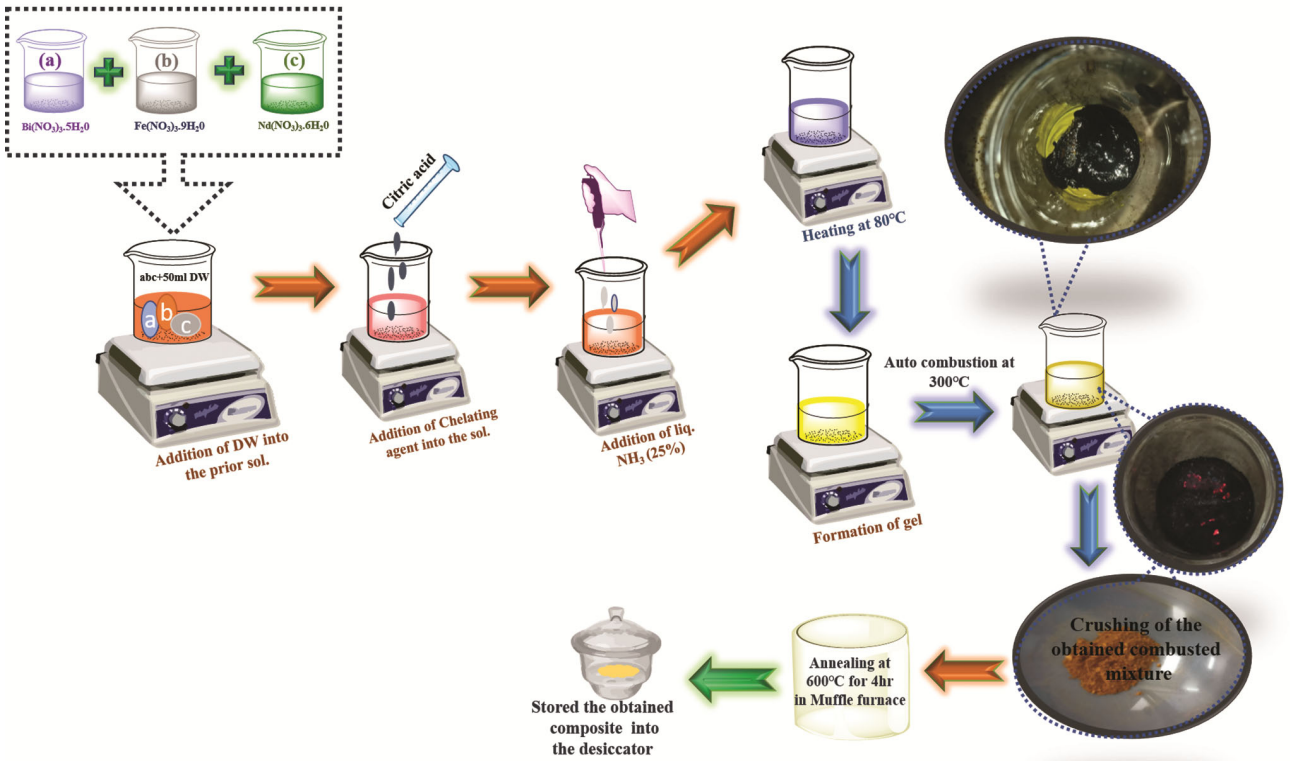


Fig. 1— Schematic representation of synthesis route of ($Bi_{1-x}Nd_xFeO_3$, x=0, 0.03, 0.06, 0.09, 0.12) nanoparticles.

Table 1 — Lattice parameters, Crystallite Size, interplanar spacing, and dislocation density, calculated with the help of XRD data.

| Sample | a=b (Å) | c (Å) | D (nm) | $d_{hkl}$ (nm) | δ |
|---|---|---|---|---|---|
| $BiFeO_3$ | 5.532 | 13.70 | 14.12 | 2.66 | 0.0087 |
| $Bi_{0.97}Nd_{0.03}FeO_3$ | 5.537 | 13.78 | 13.98 | 2.66 | 0.0090 |
| $Bi_{0.94}Nd_{0.06}FeO_3$ | 5.548 | 13.83 | 11.12 | 2.65 | 0.0102 |
| $Bi_{0.91}Nd_{0.09}FeO_3$ | 5.563 | 13.89 | 9.68 | 2.63 | 0.0113 |
| $Bi_{0.88}Nd_{0.12}FeO_3$ | 5.569 | 13.91 | 9.87 | 2.63 | 0.0145 |

phase. Additional peaks observed at approximately 28° and 28.5° were attributed to the secondary phases $Bi_2Fe_4O_9$ and $Bi_{25}FeO_{40}$, respectively[5].

The calculated values are presented in Table 1.

Figure 2 illustrates the XRD patterns of pure BFO and Nd substituted BFO samples with varying Nd doping concentrations.All XRD patterns correspond to a rhombohedral phase (JCPDS File No. 71-2494) with a combination of R3c and Pbnm space group[7]. Incontrovertibly, the Nd substitution has not significantly altered the crystallographic symmetry. The gradual increase in the dislocation density is observed with the increasing concentration of Nd in the sample,the difference in size between the host cation and the substitute cation causes lattice strain,

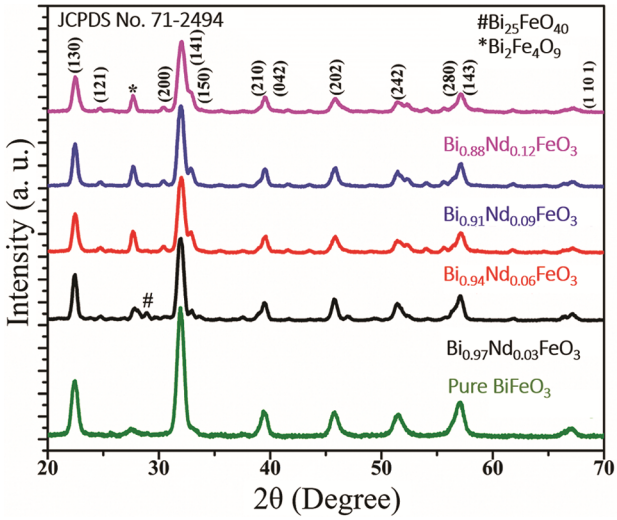


Fig. 2 — X-ray diffraction (XRD) Pattern of ($Bi_{1-x}Nd_xFeO_3$, x= 0, 0.03, 0.06, 0.09, 0.12) nanoparticles at room temperature.

which accounts for the observed effect[8]. As shown in Table 1, Crystal size is diminished because this strain distorts the local structure and slows down the nucleation process.Similar lattice strain phenomena have been exhaustively documented at the nanoscale for numerous metal oxide nanoparticles. With an increase in the concentration of Nd in the sample,

secondary phases become significant and may disrupt the crystal structure as the concentration of Nd is increased further.

### 3.2 HRTEM (High Resolution Transmission Electron Microscopy)

Image J software was utilized to make the determination of the average particle sizes of the synthesized NPs and the findings are listed in Table 2, the morphology of the NPs is found to be distorted rhombohedral which can clearly seen in the Fig. 3 (a-e) of $Bi_{1-x}Nd_xFeO_3$ (x= 0, 0.03, 0.06,0.09, 0.12) NPs.

### 3.3 ESR (Electron Spin Resonance)

The magnetic properties of nanoparticles (NPs) are influenced by several magnetic factors, including super-exchange interactions, magnetic anisotropy, spin-spin relaxation, and dipolar interactions[9]. These factors can be analyzed by examining parameters such as $g_{eff}$, resonance field, and line width, which were calculated based on the graph obtained and are presented in Table 2.

Figure 4 illustrates the ESR spectra of $Bi_{1-x}Nd_xFeO_3$ (x= 0, 0.03, 0.06, 0.09, 0.12) at ambient temperature. Each sample possesses a singular, intense signal with an asymmetrical line profile. As the $Nd^{3+}$ concentration increases from 0.03 to 0.12, the ESR lines are observed to shift to the right. This shift indicates a decrease in g-value as a consequence of an inclination in $Nd^{3+}$ concentration in the samples. Using the appropriate formula, the g-values were determined to be greater than 2 for all samples. This indicates that the samples are ferromagnetic[10]. Additionally, when x increased from 0.03 to 0.12, the line width widened from H=1659 to 1800 G (after the dopant was added). This indicates that when $Nd^{3+}$ doping concentration increases, the total number of spins participating in narrow lines decreases. Similar to VSM, when saturation magnetization decreases, the EPR data show a widening of the line and a strengthening of the peak.

Table 2 — Representation of different parameters obtained from ESR graph like$g_{eff}$, Resonance field, Line width, Center of Resonance

| Sample | $g_{eff}$ | $H_r$ (G) | $\Delta H_{PP}$ (G) | $\Delta H_{1/2}$ (G) |
|---|---|---|---|---|
| $BiFeO_3$ | 2.583 | 2670.19 | 1932.48 | 3347.15 |
| $Bi_{0.97}Nd_{0.03}FeO_3$ | 2.480 | 2780.87 | 1659.724 | 2874.726 |
| $Bi_{0.94}Nd_{0.06}FeO_3$ | 2426 | 2842.70 | 1713.73 | 2968.26 |
| $Bi_{0.91}Nd_{0.09}FeO_3$ | 2.420 | 2850.05 | 1800.60 | 3118.73 |
| $Bi_{0.88}Nd_{0.12}FeO_3$ | 2.412 | 2858.70 | 1800.34 | 3118.28 |

### 3.4 VSM (Vibrating Sample Magnetometer)

In accordance with Figure 5(a), $Bi_{1-x}Nd_xFeO_3$(x= 0, 0.03, 0.06, 0.09, 0.12)NPs exhibited symmetric M-H loops, guides that they were composed of magnetically ordered substances. The $M_r$ for x= 0.09, 0.12, 0.368, and 0.312 emu/g, respectively, increased as Nd concentration increased. The inclination in Mr value with the doping of Nd is probably because ongoing disintegration of the space-modulated spin structure of Nd-doped Bismuth Ferrite NPsand the trend of $M_s$ and $M_r$ of the samples with increasing concentration of Nd doping is clearly demonstrated in Fig. 5(c)[11,12]. As the findings of the M-H loop are well written in Table 3, the $M_s$ and $M_r$ decrease rapidly from pure BFO

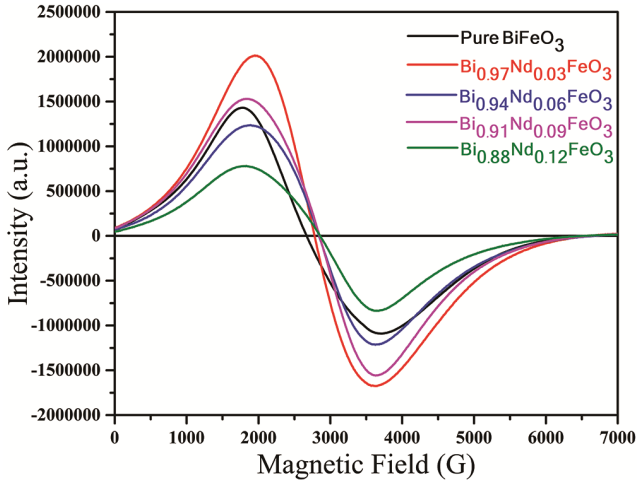


Fig. 4 — illustrates the Electron Spin Resonance (ESR) spectra of $Bi_{1-x}Nd_xFeO_3$ (x= 0, 0.03, 0.06, 0.09, 0.12) at ambient temperature. Each sample possesses a singular, intense signal with an asymmetrical.

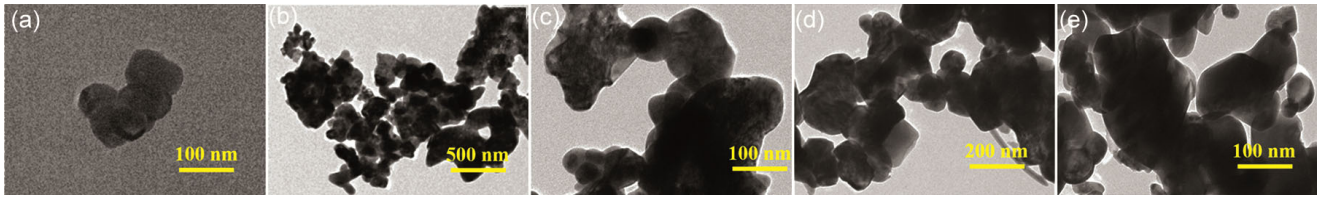


Fig. 3 — High-Resolution Transmission Electron Microscopy (HRTEM) images of $Bi_{1-x}Nd_xFeO_3$ (a) x= 0, (b) x = 0.03, (c) x = 0.06, (d) x = 0.09, & (e) x = 0.12) respectively.

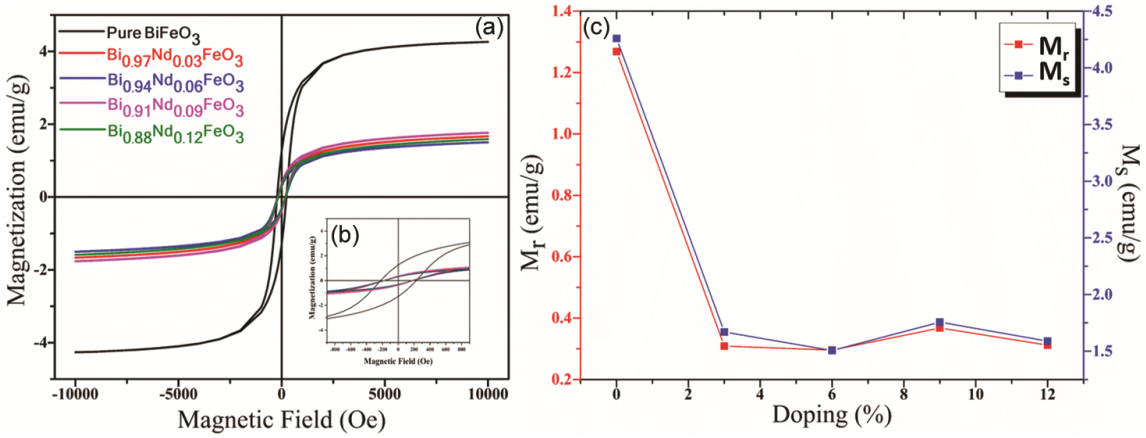


Fig. 5 — (a) M-H loop of ($Bi_{1-x}Nd_xFeO_3$, x= 0, 0.03, 0.06, 0.09, 0.12) nanoparticles, (b) Enlarged image of M-H loop to demonstrate the ferromagnetic character of the samples, & (c) Graphical presentation of variation of $M_r$ (Remanent Magnetization) and $M_s$ (Saturation Magnetization) with increasing concentration of Nd.

Table 3 — Representation of different parameters obtained from M-H graph like Saturation magnetization, Remanent magnetization, Coercivity and Squareness

| Sample | $M_s$ emu/g | $M_r$ emu/g | $H_c$ Oe | Squareness |
|---|---|---|---|---|
| $BiFeO_3$ | 4.259 | 1.268 | 222.73 | 0.2971 |
| $Bi_{0.97}Nd_{0.03}FeO_3$ | 1.669 | 0.309 | 168.23 | 0.1851 |
| $Bi_{0.94}Nd_{0.06}FeO_3$ | 1.506 | 0.296 | 184.57 | 0.1965 |
| $Bi_{0.91}Nd_{0.09}FeO_3$ | 1.756 | 0.368 | 187.13 | 0.2084 |
| $Bi_{0.88}Nd_{0.12}FeO_3$ | 1.589 | 0.312 | 174.82 | 0.1963 |

to the further doped NPs but do not vary widely with the doped samples. Because of this, the long-range AFM order is regularly disrupted at the particle surface, and the spiral spin structure has a period length of 62 nm that is partially repressed. Particle size decreases result in a rise in the ratio of surface area to volume[13]. The samples of smaller crystallite size become super paramagnetic due to electron exchange coupling[12]. Due to their decreased size, these particles are superparamagnetic between x=0.03 and x=0.12 Particles that are super paramagnetic have low coercivity/retentivity and significant magnetism. Massive amounts of uncompensated $Fe^{3+}$ ions spin at the particle's surface, thereby destroying the spin-cycloidal structure, which explains the high magnetization of the prepared samples[14,15].

## 4 Conclusion

The ($Bi_{1-x}Nd_xFeO_3$, x= 0, 0.03, 0.06, 0.09, 0.12) nanoparticles were synthesized using Pechini's modified sol-gel route followed by auto combustion method. The prepared specimens were analyzed by XRD for structural analysis, confirming the crystalline nature of the pulverized samples and depicting single phase distorted rhombohedral structures with both R3c and Pbnm space groups. The average particle size is determined with HRTEM and found to be between 18 and 50 nm. The magnetic characteristics were analyzed using M-H and ESR graphs, which reveal unambiguous relationships between the results of the two techniques. The decrease in Mr, Ms, and Hc is observed as the $Nd^{3+}$ content in the prepared nanoparticles increases, as a result of the superparamagnetic behavior of the NPs as the level of doping increases. With a reduction in saturation magnetization, both the line width and signal intensity increase. With these findings, the AFM nature of these materials can be utilized in ME devices, and since spin interaction plays a significant role, these materials can also be utilized in spintronics. Based on our findings, further research can be conducted on these nanoparticles for photocatalysis and gas sensing applications.

## References

1 Iorgu A I,Maxim F,Matei C, Ferreira L P,Ferreira P, Cruz M M, and Berger D, *J Alloys Compd*, 629(2015)62.

2 Preethi A Joana, Sharmili T, Vigneshwaran J, Jose S P, and Ragam M, *Mater Sci Eng B*, 290(2023)116296.

3 Jain P, Shankar S, & Thakur O P, *Mater Today Proce*, 67(2022)742.

4 Irandoust RandGholizadeh A, *Solid State Sci*, 101(2020) 106142.

5 Sahu A K, Satpathy S K, Rout S K, and Behera B, *Trans Electr Electron Mater*, 21(2020)217.

6 Sati P Chandra, Arora M, Chauhan S, Kumar M, and Chhoker S, *J Phys Chem Solids*, 75(2014)105.
7 Gaur A, Singh P, Choudhary N, Kumar D, Shariq M, Singh K, Kaur N, and Kaur D, *Phys B Condens Matter*, 406(2011)1877.
8 Sharma S, Kumar A & Thakur O P, *J Mater Sci: Mater Electron*, 34(2023)2050.
9 Shankar S, Maurya I, Raj A, Singh S, Thakur O P, *Appl Phys A*, 126(2020)686.
10 L Phor, and V Kumar, *J Adv Ceram*, 9(2020)243.
11 Kumar P and Kar M, *Phys B Condens Matter*, 448(2014)90.
12 Kumar M, Shankar S, Parkash O, Thakur O P, *J Mater Sci: Mater Electron*, 25(2014)888
13 Hernández N, González-González V A, Dzul-Bautista I B, Gutiérrez J, Barandiarán J M, Larramendi I Ruiz De, Cienfuegos-Pelaes R F, and Ortiz-Méndez U, *J Alloys Compd*, 638(2015)282.
14 Kumar K S, RamuS, Sudharani A, Ramanadha M, Murali G, and VijayalakshmiR P, *Phys E Low-Dimensional Syst Nanostructures*, 115(2020)113689.
15 Gautam A, Singh K , Sen K, Kotnala R K, and Singh M, *Mater Lett*, 65(2011)591.